Journal of Environmental Chemical Engineering 12 (2024) 114006

Contents lists available at ScienceDirect

Journal of Environmental Chemical Engineering

journal homepage: www.elsevier.com/locate/jece

# Removal of per- and polyfluoroalkyl substances (PFAS) from water using magnetic cetyltrimethylammonium bromide (CTAB)-modified pine bark

Ruichi Zhang [a,*], Zhongfei Ren [a], Ulrich Bergmann [b], Jean Noel Uwayezu [c], Ivan Carabante [c], Jurate Kumpiene [c], Tore Lejon [c,d], Ilil Levakov [e], Giora Rytwo [e,f], Tiina Leiviskä [a]

[a] Chemical Process Engineering, University of Oulu, P.O. Box 4300, Oulu FIN-90014, Finland
[b] Department of Biochemistry and Biocenter, University of Oulu, Oulu FIN-99020, Finland
[c] Waste Science and Technology, Luleå University of Technology, Luleå, Sweden
[d] Department of Chemistry, UiT-The Arctic University of Norway, Norway
[e] Environmental Physical Chemistry Lab, MIGAL-Galilee Research Institute, Israel
[f] Department of Environmental Sciences, Tel Hai College, Upper Galilee, Israel

ARTICLE INFO

*Keywords:*
PFAS removal
Magnetite nanoparticles
Cationic surfactant
Adsorption kinetics
Adsorption isotherm

ABSTRACT

Per- and polyfluoroalkyl substances (PFAS) have gained global attention in recent years due to their adverse effect on environment and human health. In this study, a novel and cost-effective sorbent was developed utilizing forestry by-product pine bark and tested for the removal of PFAS compounds from both synthetic solutions and contaminated groundwater. The synthesis of the adsorbent included two steps: 1) loading of cetyltrimethylammonium bromide (CTAB) onto the pine bark and followed by 2) a simple coating of magnetite nanoparticles. The developed sorbent (MC-PB) exhibited 100 % perfluorooctanoic acid (PFOA) and perfluorooctanesulfonic acid (PFOS) removal from synthetic solution (10 μg/L PFOA and PFOS) and enabled quick magnetic separation. A rapid removal of PFOA (> 80 %) by MC-PB was observed within 10 min from synthetic PFOA solution and the adsorption equilibrium was reached within 4 h, achieving > 90 % removal of PFOA (dosage 2 g/L, PFOA 10 mg/L, initial pH 4.2). The PFOA adsorption kinetics fitted well to an optimized pseudo-order model ($R^2$=0.929). Intra-particle diffusion and Boyd models suggested that the adsorption process was not governed by pore diffusion. The maximum PFOA adsorption capacity was found to be 69 mg/g and the adsorption isotherm was best described by the Dual Mode Model ($R^2$=0.950). The MC-PB demonstrated > 90 % PFOA and PFOS removal from contaminated groundwater. Furthermore, both short- and long-chain perfluorosulfonic acids and 6:2 fluorotelomer sulfonate were efficiently removed resulting in 83.9 % removal towards total PFAS (2 g/L dosage).

## 1. Introduction

Per- and polyfluoroalkyl substances (PFAS) are a diverse group of man-made fluorinated organic chemicals that have been produced since the 1940s [1]. PFAS show high chemical stability due to the strong C-F bond. Additionally, the fluorinated alkyl chain provides the compounds with good hydrophobicity and lipophobicity. These unique properties make PFAS desirable for use in a wide range of consumer and industrial products such as nonstick cookware, water-repellent clothing, fire-fighting foams, stain resistant fabrics, food contact papers, etc. [2]. However, PFAS are considered as “forever chemicals” because of their long half-life in the environment. Their mass production and widespread use have resulted in an extensive release of PFAS into the soil, air and water, which has been raising global concern due to their toxicity, persistence and bioaccumulative potential [3]. Previous studies had shown that some serious health problems were associated with exposure to PFAS compounds [4]. Therefore, the development of effective approaches to remove PFAS from an aquatic environment has become essential.

Current treatment techniques include membrane filtration [5], coagulation, adsorption [6], biological treatment [7] and advanced oxidation and reduction processes [8,9]. As an effective and convenient operation method, the adsorption of PFAS from the water matrix has attracted continuous attention owing to its wide applicability, cost-effectiveness and ease of operations. A diverse array of sorbents such as biochar [10,11], activated carbon [12], resins [13], clay

* Corresponding author.

https://doi.org/10.1016/j.jece.2024.114006
Received 25 February 2024; Received in revised form 31 July 2024; Accepted 30 August 2024
Available online 2 September 2024

materials [14] and covalent organic frameworks (COFs) [15] have been used for PFAS removal. However, the high costs and regeneration expenses of some adsorbents limit their widespread applications. Therefore, the development of cost-effective bio-based adsorbents for PFAS removal have received increasing attention in recent decades. Various materials, including bark chips [16], quaternized cotton [17] and aminated rice husk [18] have been used for PFAS removal. These bio-based materials are normally cheap, abundant and require less processing, and thus can be promising alternatives to costly commercial sorbents. However, raw bio-based sorbents usually show inadequate adsorption of PFAS. Hence, grafting raw biomass with different functional groups (e.g. amine group, quaternary ammonium group, hydrophobic chains) has been performed to enhance their adsorption ability for PFAS compounds [18]. After the adsorption treatment, filtration and sedimentation can be used to separate the exhausted sorbents from the treated water. In recent years, as an alternative, magnetic nanomaterials have been investigated by many researchers due to their quick and effective magnetic separation property in wastewater treatment processes. Many studies have reported the effectiveness of synthesized magnetic biosorbents for the removal of heavy metals [19,20], antibiotics [21] and dyes [22,23] from water. Park et al. reported that magnetic anion-exchange resin achieved good settleability in PFAS removal [24].

In this study, a novel composite, magnetite coated cetyltrimethylammonium bromide (CTAB) pine bark (MC-PB) was synthesized and used for PFAS removal from both synthetic PFAS solutions and contaminated groundwater. The modification was first conducted by loading CTAB onto the pine bark particles followed by a simple magnetite coating (with $Fe^{3+}$ and $Fe^{2+}$) process. The cationic surfactant CTAB introduced onto the sorbent facilitates its adsorption ability towards various water pollutants through hydrophobic and electrostatic interactions. Moreover, the magnetism allows rapid sorbent separation from water. To the best of our knowledge, this is the first study to report the two-step modification (CTAB impregnation followed by magnetite coating) of a sorbent used for PFAS removal. The adsorption behaviour towards PFAS was investigated by means of batch tests using synthetic PFAS solutions. The adsorption kinetics and isotherms of PFOA were studied. Different characterization techniques were applied to investigate the properties of the synthesized sorbent before and after the adsorption experiment. Finally, the adsorption performance of the prepared sorbent towards different PFAS in real groundwater was investigated.

## 2. Materials and methods

### 2.1. Raw materials and chemicals

The raw pine bark (raw PB) was collected from the RoihuPuu Oy (Oulu, Finland) and dried at 80 ℃ for 24 h and then sieved to obtain a 90–250 μm fraction for further use. Cetyltrimethylammonium bromide (CTAB, >99 %) was purchased from ACROS Organics. Iron (III) chloride hexahydrate ($FeCl_3 \bullet 6H_2O$, >99 %, ACROS Organics) and iron (II) sulfate heptahydrate ($FeSO_4 \bullet 7H_2O$, >99 %, J.T. Baker) were used for magnetic component impregnation. Perfluorooctanoic acid (PFOA, $C_7F_{15}COOH$, >95 %) and perfluorooctanesulfonic acid (PFOS) were purchased from Sigma-Aldrich. NaOH (ACROS Organics) and HCl (37 %, Merck) were used for pH adjustment. All chemicals used in this study were of analytical grade. The groundwater was sampled from an area near a hotspot where PFAS-containing film forming foams (FFF) had been used in firefighting training activities.

### 2.2. Synthesis of MC-PB pine bark

Firstly, CTAB modification was made by adding 250 mL of CTAB solution (12 g/L) to 10 g of pine bark (pine bark: CTAB=1:0.3 w/w). Then the solution was mixed in a horizontal rotary shaker for 48 h at room temperature. Next, the mixture was filtered and washed with tap water to remove the unreacted reagent. The obtained CTAB-modified pine bark was then dried in an oven at 60 ℃ for 24 h, after which it was ready to be used for the subsequent magnetic component impregnation. Briefly, 6 g of CTAB-modified pine bark was dispersed in 200 mL ultrapure Milli-Q water and the solution was mixed using a magnetic stirrer. Then 6.43 g of $FeCl_3 \bullet 6H_2O$ and 3.34 g of $FeSO_4 \bullet 7H_2O$ ($Fe^{3+}$: $Fe^{2+}$=2:1) were dissolved in 60 mL of ultrapure Milli-Q water. Thereafter, the mixed iron solution and NaOH (1 M) were added dropwise to the dispersed pine bark solution during agitation, and the pH was maintained in the range of 9–10. The mixture was then heated up to 80 ℃ and stirred for 3 h. Upon completion of the reaction, the solution was cooled down to room temperature and the solid product (MC-PB) was filtered using vacuum filtration and washed with tap water. The obtained product was then dried in the oven at 60 ℃ for 24 h. To identify the synthesized magnetic particles in this study, the magnetic modification was repeated in the absence of CTAB-modified pine bark. The synthesized pure magnetic particles were then characterized by XRD and TEM analysis. Additionally, the magnetic pine bark (magnetic PB) was also synthesized without CTAB modification to compare its PFOA adsorption behaviour with that of MC-PB (adsorption conditions: dosage 4 g/L, initial PFOA concentration 10 mg/L, contact time 24 h). It should be noted that no significant change in the size of the sorbent was observed after CTAB modification.

### 2.3. PFOA removal with MC-PB

#### 2.3.1. Effect of solution pH

PFOA removal with MC-PB was conducted in batch mode at room temperature. The sorbent (2 g/L) was weighed into 15 mL VWR centrifuge tubes and 10 mL of PFOA solution (10 mg/L) was added. A concentration of 10 mg/L PFOA solution was selected because PFOA concentration in polluted water can range from ng/L to several mg/L [25]. The pH of the PFOA solution was adjusted in the range of 4.0–11.0. The tubes were shaken for 24 h in a Fisherbrand tube rotator. All experiments were conducted in duplicate. After the adsorption experiment, the supernatant was separated with a magnet. It is worth noting that, in real-world applications, the separation of the sorbent will depend on its weight and how the sorbent is applied. These factors should be carefully designed and evaluated before practical implementation. PFOA concentration was analysed using ultra-high performance liquid chromatography (Acquity UPLC System, Waters) coupled with a tandem mass spectrometer (Q ExactiveTM Plus Hybrid Quadrupole-Orbitrap 176 TM Mass Spectrometer, Thermo) (UPLC-MS). An Acquity UPLC® BEH C18 column (1.7 μm, 181 2.1 × 100 mm column, Waters) was used and operated at 50 ℃. The mobile phase A was 10 mM ammonium acetate in water and the mobile phase B was absolute methanol. The injection flow rate was set at 0.3 mL/min (volume 10 μL) at a temperature of 50 ℃. The limit of detection (LOD) was 0.1 μg/L, the limit of quantification (LOQ) was 1 μg/L. Detailed information on the PFOA and PFOS analytical methods can be found in the supplementary material (Table S1).

#### 2.3.2. Effect of contact time

PFOA removal from the aqueous solution was conducted using different contact times (10 min–72 h). A dosage of 2 g/L, an initial PFOA concentration of 10 mg/L and a solution pH of 4.2 (without adjustment) were kept constant, yielding an initial concentration of 5 mg PFOA per g sorbent. Otherwise, the adsorption procedure described in Section 2.3.1 was followed. The data were then fitted with the pseudo-first-order (PFO, Eq. S1) [26], pseudo-second-order (PSO, Eq. S2) [27], Elovich models (Eq. S3) [28], intra-particle diffusion model (Eq. S4) [29], Boyd model (Eqs. S5 and S6) [30] and the optimized pseudo-order model (Eq. S7), which arises from the integration of the kinetics rate law [31]. All the equations and descriptions can be found in Text S1.

#### 2.3.3. PFOA adsorption capacity

PFOA solutions (10–671 mg/L) were prepared without pH adjustment. Contact time (24 h) and sorbent dosage (2 g/L) were maintained constant. The adsorption procedure used was the same as described in Section 2.3.1. The PFOA adsorption capacity (q) was obtained as shown in Eq. 1:

$$q = \frac{(C_i - C_r)V}{m} \quad (1)$$

where $C_i$ (mg/L) and $C_r$ (mg/L) are the initial PFOA concentration and the residual PFOA concentration in solution, $V$ (L) is the solution volume and m (g) is the adsorbent weight.

The acquired data was fitted to the non-linear two-parameter isotherm form of the Langmuir (Eq. S8) and Freundlich (Eq. S9) models, and the non-linear three-parameter form of Redlich-Peterson (Eq. S10) and Dual Mode models (Eq. S11). The latter was developed from the Langmuir equation by adding a partition factor [32] that reflects the affinity of the adsorbate to the sorbent. All the equations are described in Text S2.

Additionally, considering environmentally realistic concentrations of PFAS, adsorption tests (dosage 2 g/L) were performed in single systems (PFOA and PFOS) and co-existing systems (PFOA+PFOS) at low concentrations (10 μg/L and 100 μg/L).

#### 2.3.4. PFOA removal from real groundwater

To evaluate the efficiency of MC-PB for PFAS removal in real cases, groundwater contaminated with PFAS was used for the batch adsorption experiment. A dosage of 2 g/L MC-PB was weighed and subsequently mixed with 250 mL of sampled groundwater in bottles. The mixture was subjected to a rotary mixer for 12 h at room temperature to ensure sufficient time for reactions between PFAS and the sorbent. The adsorption test was done in duplicate. After the experiment, the supernatant was separated from the sorbent with a magnet. The concentration of PFAS compounds in the groundwater before and after the adsorption test was analysed by Eurofins Food & Feed Testing Sweden AB with German standard method DIN 38407–42 using high performance liquid chromatography and mass spectrometric detection (HPLC/MS-MS) after solid-liquid extraction.

### 2.4. Characterization methods

Raw PB, MC-PB and PFOA-treated MC-PB (initial PFOA concentration 100 mg/L) were characterized by X-ray photoelectron spectroscopy (XPS) and Fourier transform infrared (FTIR) spectroscopy. XPS was performed on a Thermo Fisher Scientific ESCALAB 250xi instrument with a monochromatic Al Kα source (1486.6 eV). The charge calibration was done by setting the binding energy of adventitious carbon to 284.8 eV. FTIR spectra were acquired in the 400–4000 $cm^{-1}$ wavenumber range using a Bruker Vertex V80 vacuum FTIR spectrometer, and the recorded spectra were visualized using the OPUS program. The synthesized pure magnetic particles, MC-PB and PFOA-treated MC-PB, were characterized using X-ray diffraction (XRD) performed using a Rigaku Smartlab rotating anode diffractometer with Co Kα radiation. The morphology and elemental distribution of the samples were analysed using an energy-filtered transmission electron microscope (JEOL JEM-2200FS EFTEM/STEM (scanning transmission electron microscopy)) equipped with a JEOL Dry SD100GV energy dispersive X-ray spectroscopy (EDS) detector and field emission scanning electron microscope (FESEM).

## 3. Results and discussion

### 3.1. PFOA removal studies

The magnetic PB achieved a PFOA removal efficiency of 15 % ±0.1 %, which was much lower compared to MC-PB (87.9 %±0.8 %) under the same adsorption conditions (dosage 4 g/L, initial PFOA concentration 10 mg/L, contact time 24 h), confirming that CTAB modification played an essential role in the PFOA adsorption process.

#### 3.1.1. Effect of solution pH

The effect of the solution pH on the PFOA removal efficiency of MC-PB is shown in Fig. 1 (a). The highest removal efficiency (94.6 %±0.7 %) was achieved at pH 4. At the initial pH of the PFOA solution (pH 4.2, PFOA concentration 10 mg/L), the removal efficiency was 90.5 % ±1.1 %. PFOA removal efficiency (80.9–91.6 %) was relatively stable in the pH range of 5.0–9.0. It has been reported that hydrophobic interaction is not sensitive to changes in pH [1], and this is in accordance with the results in this study that there was no substantial difference in PFOA removal in the pH range of 4–9. With a further increase in pH from 10 to 11, the PFOA removal efficiency dramatically decreased from 57.2 %±0.7 to 30.0 %±3.2, which was attributed to higher $pH_{pzc}$ value of the CTAM-modified sorbent [33].

#### 3.1.2. Effect of contact time and adsorption kinetics

The effect of contact time on PFOA removal by MC-PB is presented in Fig. 1(b). A rapid removal of PFOA (>80 %) was observed in the first 10 min. Then the removal efficiency increased to 92.7 %±0.5 % within 4 h and remained stable in the range of 92.7 %-95.3 % with further contact time (4h-72h). Equilibrium was reached after 4 h. The adsorption kinetics were investigated by the non-linear pseudo-first-order (PFO), pseudo-second order (PSO) Elovich, and optimized pseudo-order (OPO) (Fig. 2 (a)) models. The $q_e$ (mg/g) obtained from the PFO, PSO and OPO models (Table 1) was close to the experimental data (5.0 mg/g), but the fit of PFO and PSO, as can be observed from the determination coefficient ($R^2$), is not good. Elovich model showed a reasonable fit to the data. The model has been extensively applied to chemisorption reactions [28]. However, the best fit from those models was obtained by the optimized pseudo-order model ($R^2$=0.929). Intra-particle diffusion and the Boyd model were applied to the data to further understand the adsorption behaviour. The linear plot of $q_t$ versus $t^{½}$ with a zero intercept indicates that the adsorption process is controlled by intra-particle diffusion. In this study, the plot of $q_t$ versus $t^{½}$ exhibited two regions (Fig. S1 (a)). The first linear region indicates film diffusion, while the second region typically suggests intra-particle diffusion. However, the second region in the present study presented very poor linearity and the value of $q_t$ remained quite stable with an increased $t^{½}$. These results suggested that the adsorption process was not controlled by intra-particle diffusion and that film diffusion may play a more important role in adsorption behaviour. The Boyd model could help to predict the rate-limiting step of the adsorption process, e.g. if the plot of $B_t$ versus time t is in linear form and passes through the origin, then internal diffusion is considered to be the rate-limiting step [34]. The Boyd plot in this study was not linear and did not pass through the origin (Fig. S1 (b)). This indicated that intra-particle diffusion was not the rate-limiting step.

#### 3.1.3. Adsorption isotherms

The maximum adsorption capacity of MC-PB was determined to be 69 mg/g and it exhibited an increase with the PFOA concentration. This phenomenon can be attributed to the stronger driving force between the sorbent and sorbate at a higher PFOA concentration. Subsequently, the data was fitted to the non-linear Langmuir two-parameter isotherms, i.e. Langmuir and Freundlich, and non-linear three-parameter isotherms, i-e- Redlich-Peterson and Dual Mode (Fig. 2 (b)). The Redlich-Peterson model was found to provide relatively good fit to the experimental data in terms of the highest $R^2$ (0.930) and lowest $\chi^2$ value (Table S2). According to this model, if the exponent g value is close to unity, the adsorption is compatible with the Langmuir model rather than the Freundlich model [35]. In this study, the g value (0.622) was not close to

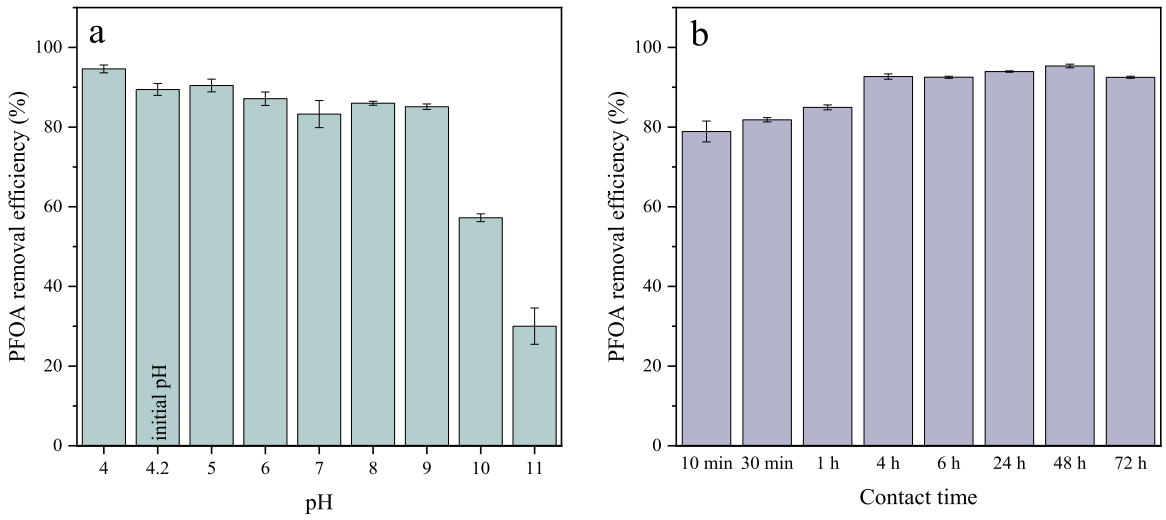


**Fig. 1.** Effect of solution pH (a) and contact time (b) on PFOA removal efficiency onto MC-PB (dosage 2 g/L; initial PFOA concentration 10 mg/L; temperature 21 ℃; contact time 24 h (for effect of pH experiment); initial solution pH 4.2 (for effect of solution pH experiment); error bars represent the range of two replicates).

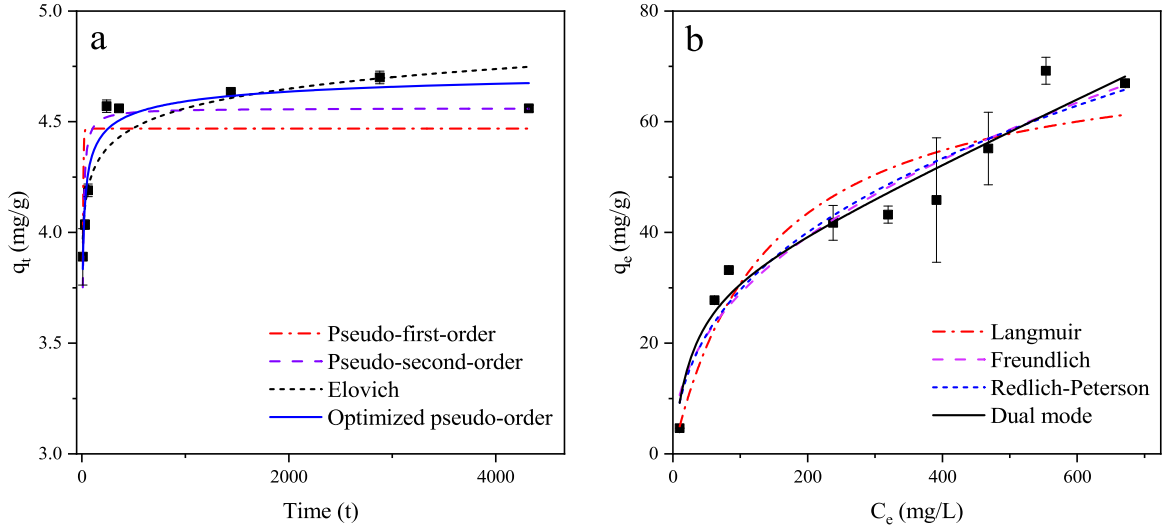


**Fig. 2.** Adsorption kinetics (a) and isotherms (b) by non-linear models for PFOA removal onto MC-PB (dosage 2 g/L; pH initial 4.2; initial PFOA concentration 10 mg/L (for kinetics); initial PFOA concentration 10—671 mg/L (for isotherm); temperature 21 ℃; error bars represent the range of two replicates).

unity. The result indicated that the adsorption process may not occur at a homogenous surface. However, it should be noted that the best fit was obtained for the three-parameter Dual Mode model ($R^2$=0.950), which is based on a combination of the Langmuir mechanism that is significant mostly at low adsorbed amounts, and a partition mechanism between the solvent and sorbent, which becomes significant at larger equilibrium concentrations [36,37]. This suggests that the adsorption mechanism is based on such a combination. However, the variations in the repeats around concentrations of 400 mg/L and 500 mg/L were relatively large, and overall, none of these models provided a perfect fit to the adsorption isotherm. Moreover, typically the adsorption mechanisms cannot be directly determined based on theoretical adsorption models; instead, other mechanistic adsorption models have to be used in combination with analytical characterization techniques [35,38]. PFOS removal reached 100 % at a lower initial concentration (10 μg/L and 100 μg/L) in both single and co-existing systems (Table S3). The removal efficiency of PFOA was 100 % at an initial concentration of 10 μg/L in both systems; the removal efficiency slightly decreased to 98 % when the initial concentration was increased to 100 μg/L. The results suggested that MC-PB can remove PFOA and PFOS efficiently at environmentally realistic concentrations.

### 3.1.4. *PFAS removal from real groundwater*

The groundwater mainly contained perfluorosulfonic acids (PFSAs, C4—C8) and perfluorocarboxylic acids (PFCAs, C4—C8). In addition, 6:2 fluorotelomer sulfonate (6:2 FTS) was detected. Other long-chain PFSAs and PFCAs (C>9) existed in small amounts (< 10 ng/L). The distribution of the main PFAS in raw groundwater, and the concentrations of the PFAS compounds in the groundwater before and after the adsorption test are listed in Table 2. Perfluorohexanesulfonic acid (PFHxS) was the most abundant species in the groundwater, accounting for over 50 % of the total PFAS concentration. Next, noticeable amounts of PFBS, PFPeS, PFHxA and PFOA were observed in the range of 1200—1900 ng/L. The PFAS removal efficiency from groundwater by MC-PB is presented in Fig. 3. High removal efficiency (>80 %) was achieved for most of the PFAS. The MC-PB was efficient in removing both short- and long-chain PFSAs with removal efficiency in the range of 77.9—99.5 %. The sorbent also showed good removal efficiency (81.0—90.8 %) towards long-chain PFCAs (C7 and C8), whereas inadequate adsorption ability was observed towards short-chain PFCAs (C4

**Table 1**
Parameters of the PFO, PSO, Elovich, intra-particle diffusion and Boyd models.

| Models | Parameters | MC-PB |
|---|---|---|
| Pseudo-first-order | $k_1$ (1/min) | 0.201 |
| | $q_e$ (mg/g) | 4.469 |
| | $R^2$ | 0.449 |
| | $\chi^2$ | 0.082 |
| Pseudo-second-order | $k_2$ (g/mg × min) | 0.102 |
| | $q_e$ (mg/g) | 4.561 |
| | $R^2$ | 0.784 |
| | $\chi^2$ | 0.033 |
| Elovich | α (mg/(g×min)) | 3.756E+11 |
| | β (g/mg) | 7.810 |
| | $R^2$ | 0.845 |
| | $\chi^2$ | 0.023 |
| Optimized pseudo-order | $k_a$ (depending on $n_a$) | 0.0349 |
| | $n_a$ (dimensionless) | 4.068 |
| | $q_e$ (mg/g) | 4.811 |
| | $R^2$ | 0.929 |
| | $\chi^2$ | 0.011 |
| Intra-particle diffusion | $k_{i,1}$ (mg/g × $min^{½}$) | 0.055 |
| | $C_1$ | 3.737 |
| | $R_1^2$ | 0.994 |
| | $\chi_1^2$ | 3.5E−4 |

**Table 2**
PFAS concentration in the groundwater before and after adsorption onto MC-PB (dosage 2 g/L; pH 7.4; contact time 12 h; temperature 21 ℃).

| PFAS category | PFAS compound | Concentration in groundwater (ng/L) | Concentration after adsorption (ng/L) |
|---|---|---|---|
| PFSAs | PFBS (C=4) | 1400 | 310 |
| | PFPeS (C=5) | 1300 | 64 |
| | PFHxS (C=6) | 9700 | 260 |
| | PFHpS (C=7) | 65 | <0.3 |
| | PFOS (C=8) | 120 | <10 |
| PFCAs | PFBA (C=4) | 320 | 320 |
| | PFPeA (C=5) | 670 | 640 |
| | PFHxA (C=6) | 1900 | 1100 |
| | PFHpA (C=7) | 510 | 97 |
| | PFOA (C=8) | 1200 | 110 |
| 6:2 FTS | | 330 | <0.3 |
| Sum of PFAS | | 18000 | 2900 |

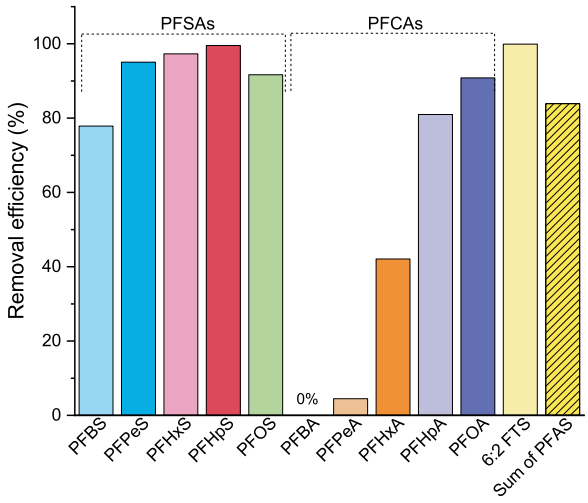


**Fig. 3.** PFAS removal efficiency from groundwater onto MC-PB (dosage 2 g/L; contact time 12 h; temperature 21 ℃).

and C5). It has been reported that PFSAs were more readily adsorbed onto the oxide surface and their adsorption capacities on other sorbents were higher than those of PFCAs with the same carbon numbers. This is probably due to the PFSAs being more hydrophobic than PFCAs (for the same chain length) [39]. In this study, it was observed that higher removal efficiency could be achieved for PFHxS compared to PFHxA by MC-PB;a similar result was reported in the case of GAC sorbent by Westreich et al. (2018). In addition, MC-PB was able to remove 99.9 % of 6:2 FTS from the groundwater. Overall, the total PFAS removal efficiency from groundwater was 83.9 % (without pH adjustment), which is comparable to some reported commercial sorbents with the same dosage (2 g/L) [40]. This suggested that use of the prepared sorbent in real applications is feasible. Future scale-up possibilities can be further evaluated through column studies and field studies.

### 3.2. Characterization of the adsorbent

#### 3.2.1. Identification of $Fe_3O_4$ particles

XRD profiles of the synthesized magnetic particle, MC-PB and PFOA-treated MC-PB are shown in Fig. 4 (a). For the synthesized magnetic particle, the main characteristic peaks observed with the HKL values of (2 2 0), (3 1 1), (4 0 0), (4 2 2), (5 1 1) and (4 4 0) correspond to the magnetite ($Fe_3O_4$) phase [41]. MC-PB and PFOA-treated MC-PB presented an amorphous form together with distinguishable $Fe_3O_4$ peaks. These findings indicated that $Fe_3O_4$ particles had successfully been introduced and stabilized on the pine bark. In addition, the successful separation of the used MC-PB from the solution was achieved by using a magnet, which confirmed the magnetism of the sorbent.

#### 3.2.2. Changes in surface functional groups

The FTIR spectra of the samples are shown in Fig. 4 (b). The broad absorption band at 3404 $cm^{-1}$ can be observed for all the samples, corresponding to the symmetric O–H stretching in general, including hydroxyl and phenolic group in bark materials [42]. Methyl ($CH_3$) and methylene ($CH_2$) groups exhibit a set of symmetric and asymmetric vibrations [43]. The broad band at approx. 2922 $cm^{-1}$ in the raw PB is ascribed to a combination of those vibrations in lignin-containing materials [44,45]. After modification, the intensity of the stretching vibrations of the $CH_2$ asymmetric and symmetric (at 2922 $cm^{-1}$ and 2851 $cm^{-1}$, respectively) bonds is enhanced, due to the large amount of methylene groups introduced by the CTAB molecules. [46]. The peak at 1606 $cm^{-1}$ belongs to the stretching vibration of the original amine group in bark materials [46]. The band at 1733 $cm^{-1}$ in the raw PB is attributed to the stretching vibration of the C=O group in the ester group present in hemicelluloses [47,48], and the peak at 1509 $cm^{-1}$ is related to the C=C stretching of the aromatic skeleton of lignin [49,50]. However, both peaks significantly decreased after modification. The bands at 1239 $cm^{-1}$ and 1204 $cm^{-1}$ were obvious after PFOA adsorption, matching the $CF_3$ and $CF_2$ groups from the adsorbed PFOA [50]. At the same time, an absorption band at 1683 $cm^{-1}$ appeared after adsorption, corresponding to the C=O vibration in carboxylic group from PFOA [51]. The differences in the FTIR spectra due to PFOA adsorption (increase of C=O and C-F bands and decrease in the C=C band) are emphasized in Fig. S2, which exhibits the spectrum of the subtraction of the modified pine bark from the PFOA-modified PB sample. The results confirmed the successful modification of CTAB onto the pine bark and its adsorption ability towards PFOA.

Further analysis of the changes in surface structure and functional groups of the adsorbent was conducted by XPS. According to the surface element compositions by XPS analysis (Table 3), the raw pine bark contained mainly carbon (79.3 %) and oxygen (20.1 %) with a small amount of nitrogen (0.58 %). After modification, the nitrogen content slightly increased, and iron was detected due to the successful grafting of the quaternary ammonium surfactant (CTAB) and magnetic particles onto the pine bark. The sample of PFOA-treated MC-PB showed a fluoride content of 14.7 %, which confirmed that PFOA was attached to the

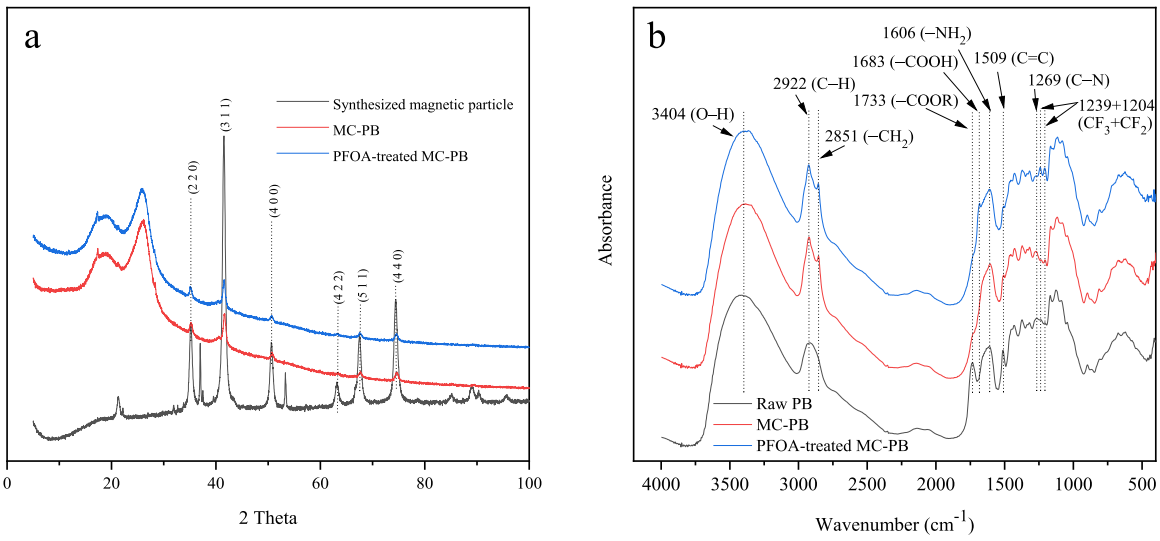


**Fig. 4.** XRD profiles (a) of synthesized magnetic particles, MC-PB and PFOA-treated MC-PB and FTIR spectra (b) of raw PB, MC-PB and PFOA-treated MC-PB.

**Table 3**
Surface composition (at.%) of raw, modified and PFOA-treated MC-PB by XPS analysis (initial concentration of PFOA=100 mg/L).

| Sample | Atomic percentage of the elements (%) | | | | |
|---|---|---|---|---|---|
| | C | O | N | Fe | F |
| Raw PB | 79.3 | 20.1 | 0.6 | - | - |
| MC-PB | 58.8 | 35.6 | 0.8 | 4.8 | - |
| PFOA-treated MC-PB | 49.4 | 29.8 | 0.8 | 5.3 | 14.7 |

MC-PB.

The C 1 s spectra of the raw PB and MC-PB could be fitted into four major peaks (Fig. 5): aromatic and aliphatic carbon (C1; C–C/C–H) at 284.8 eV; carbon single bonds with oxygen and nitrogen (C2; C–O/C–N) at 286.3 ± 0.1 eV; carbon double bonds with oxygen (C3; C=O) at 287.9 ± 0.3 eV; and C4 (O–C=O) originating from the ester group present in hemicellulose [51,52]. The C 1 s region of the PFOA-treated MC-PB was fitted into five peaks. In addition to the four above-mentioned peaks (C1–C4), a new peak C5 was observed at 291.4 eV, which was related to the C–F bond in PFOA (in C–$F_2$). Additionally, the C–F bond (in C–$F_3$) should have existed at ~294 eV in the C 1 s spectrum of PFOA-treated MC-PB, but the peak was not obvious. This is probably because the proportion of the C—F bond (in C–$F_3$) is lower than that of the C–F bond (in C–$F_2$) in PFOA. Finally, the C=O bond slightly shifted to a higher binding energy, which was probably due to the presence of a carboxylic group derived from adsorbed PFOA.

In the region of N1s spectra, the raw PB presented two peaks, at 400.1 eV and 402.1 eV (Fig. 6). The peak at 400.1 eV corresponded to the nitrogen bound to carbon in amines or amides originating from nitrogen compounds in the raw biomass [53,54]. The peak at 402.1 eV was related to the protonated amino groups (-$NH_3^+$/-$N(CH_3)_3^+$ [53]. After modification, the peak at ~402 eV was significantly enhanced, and this confirmed the presence of quaternary nitrogen [54], which can provide active binding sites for anionic pollutant adsorption through electrostatic attraction [53]. The observed quaternary nitrogen revealed the successful introduction of CTAB onto the raw PB. Moreover, the peak assigned to the quaternary nitrogen was still observed in PFOA-treated MC-PB after the adsorption process and the nitrogen content in MC-PB before and after PFOA adsorption remained unchanged (Table 3). This indicated that the introduced quaternary nitrogen groups were stable and may not have leached out during the adsorption process. The results indicated that electrostatic interactions between the anionic headgroup of PFAS and the cationic ammonium group of the MC-PB were involved in the adsorption process. The F 1 s spectrum of PFOA-treated MC-PB displayed a single peak at 688 eV (Fig. S3), which corresponds to organic fluorine bonding. This confirmed that PFOA was successfully adsorbed onto MC-PB.

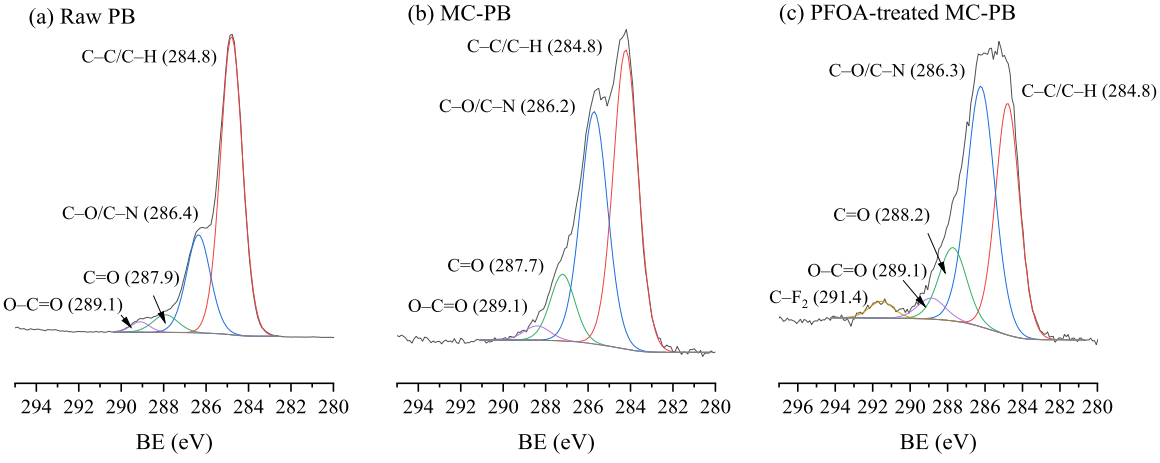


**Fig. 5.** C 1 s XPS spectra of (a) raw PB (b) MC-PB (c) PFOA-treated MC-PB.

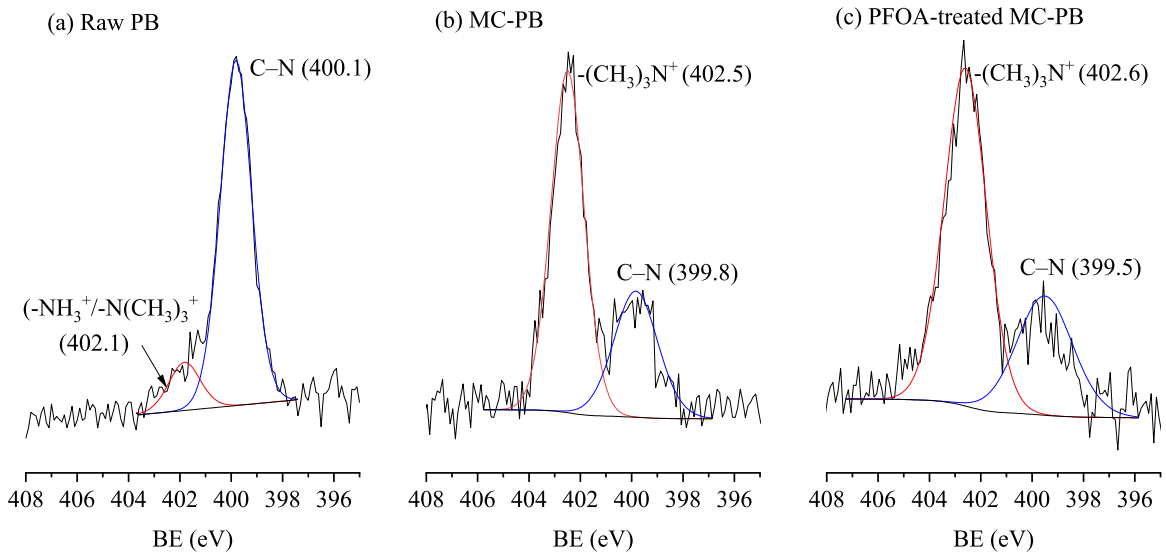


**Fig. 6.** N 1 s XPS spectra of (a) raw PB (b) MC-PB (c) PFOA-treated MC-PB.

### 3.2.3. *Morphological changes of the adsorbent*

The TEM images of a synthesized magnetic particle, MC-PB and PFOA-treated MC-PB are presented in Fig. 7. The formed magnetic particles aggregated together, and the size of the particles was approx. 3–30 nm (Fig. 7 (a)). After the modification, the TEM image revealed that the spherical shape of the magnetic nanoparticles dispersed onto the fibre-shaped surface of the MC-PB (Fig. 7 (b)), suggesting the successful introduction of the magnetic particles onto the biomass. Additionally, a film-like component was observed in PFOA-treated MC-PB (Fig. 7 (c)). According to the EDS mapping results (Fig. S4 and S5), these film-like components contained fluorine and thus indicate PFOA, whereas fluorine was not detected in the fibre-shaped material in Fig. 7 (b). PFOA has been reported to form hemi-micelles or micelles in water through the hydrophobic aggregation of C–F chains even when its concentration is in the range of 0.01–0.001 times that of CMC (3460 mg/L for PFOA) [2,55–57]. In this study, the PFOA could have accumulated on the surface of the sorbent. FESEM micrographs of the raw PB presented a relatively smoother surface with some granules attached on the surface (Fig. S6). After modification, the material displayed a coarse surface, which can be attributed to the presence of magnetite nanoparticles deposited on the surface of the pine bark. A similar observation has also been reported by Asimbaya et al.

## 4. Conclusion

The synthesized sorbent, MC-PB, was proved to be effective for PFOA and PFOS removal from synthetic solutions at environmentally realistic concentrations. The sorbent was also efficient at removing most of the PFAS from contaminated groundwater, whereas inadequate adsorption ability was observed towards short-chain PFCAs (C4 and C5). XRD and TEM analyses revealed that $Fe_3O_4$ nanoparticles were formed, and these nanoparticles were stable after PFOA adsorption. FTIR and XPS analyses confirmed the successful grafting of a hydrophobic chain (methylene chain) and quaternary ammonium group onto the pine bark. The maximum adsorption achieved towards PFOA was 69 mg/g) and high PFOA removal efficiency could be reached in a broad pH range (4–9) in the synthetic PFOA solution. Rapid PFOA removal (> 80 %) was observed within 10 min and the adsorption kinetics indicated that the process was apparently governed by film diffusion. It is suggested that hydrophobic interaction and electrostatic attraction were involved in the adsorption process. The overall removal efficiency of total PFAS from groundwater reached 83.9 %, which indicated that the MC-PB is a promising alternative for real applications. This study demonstrates the potential reuse of forestry by-product as efficient sorbent for PFAS removal, offering a sustainable solution for PFAS control. Future studies could focus on the optimization of the modification process and investigating the recycling of CTAB solution to further reduce costs in the modification stage, thereby promoting its broad applicability in real-

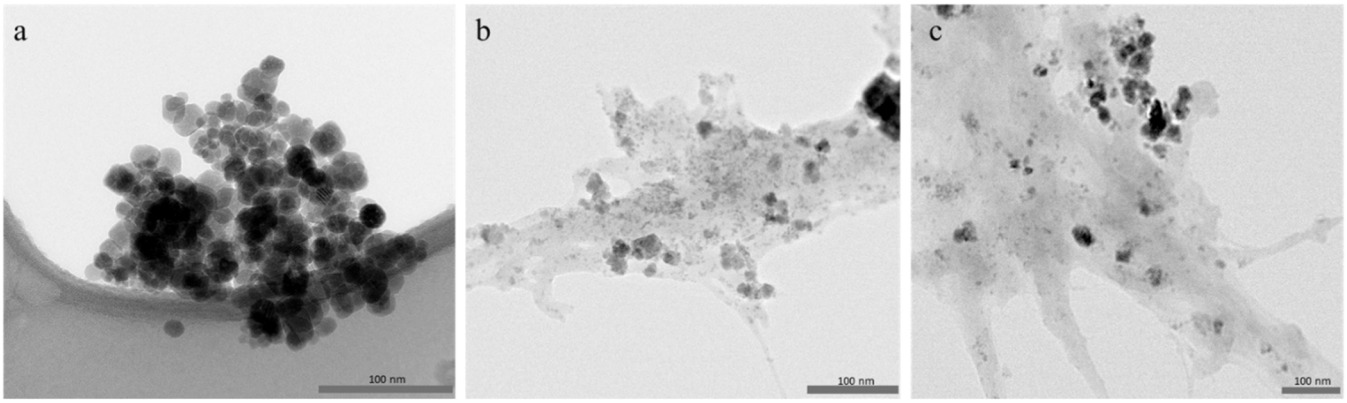


**Fig. 7.** TEM images of (a) synthesized magnetic particle (b) MC-PB (c) PFOA-treated MC-PB.

world applications.

## CRediT authorship contribution statement

**Ruichi Zhang:** Writing – original draft, Methodology, Investigation, Formal analysis, Data curation, Conceptualization. **Zhongfei Ren:** Writing – review & editing, Methodology, Investigation, Formal analysis. **Ulrich Bergmann:** Resources, Formal analysis. **Jean Noel Uwayezu:** Writing – review & editing, Resources. **Ivan Carabante:** Writing – review & editing, Resources. **Jurate Kumpiene:** Writing – review & editing, Resources. **Tore Lejon:** Writing – review & editing, Resources. **Ilil Levakov:** Writing – review & editing, Formal analysis. **Giora Rytwo:** Writing – review & editing, Formal analysis. **Tiina Leiviskä:** Writing – review & editing, Supervision, Resources, Project administration, Funding acquisition, Conceptualization.

## Declaration of Competing Interest

The authors declare that they have no known competing financial interests or personal relationships that could have appeared to influence the work reported in this paper.

## Data availability

Data will be made available on request.

## Acknowledgements

The work was financially supported from the European Union programme (Less-PFAS project: Sustainable management of PFAS-contaminated materials), and the Regional Council of Lapland, Norrbotten County Council and Troms og Finnmark County Municipality. We gratefully acknowledge the support from the Centre for Material Analysis, University of Oulu (Finland) for the material characterization.

## Appendix A. Supporting information

Supplementary data associated with this article can be found in the online version at doi:10.1016/j.jece.2024.114006.

## References

[1] D.Q. Zhang, W.L. Zhang, Y.N. Liang, Adsorption of perfluoroalkyl and polyfluoroalkyl substances (PFASs) from aqueous solution - a review, Sci. Total Environ. 694 (2019) 133606, https://doi.org/10.1016/j.scitotenv.2019.133606.
[2] Q. Yu, R. Zhang, S. Deng, J. Huang, G. Yu, Sorption of perfluorooctane sulfonate and perfluorooctanoate on activated carbons and resin: kinetic and isotherm study, Water Res. 43 (2009) 1150–1158, https://doi.org/10.1016/j.watres.2008.12.001.
[3] J.-M. Jian, D. Chen, F.-J. Han, Y. Guo, L. Zeng, X. Lu, F. Wang, A short review on human exposure to and tissue distribution of per- and polyfluoroalkyl substances (PFASs), Sci. Total Environ. 636 (2018) 1058–1069, https://doi.org/10.1016/j.scitotenv.2018.04.380.
[4] E.M. Sunderland, X.C. Hu, C. Dassuncao, A.K. Tokranov, C.C. Wagner, J.G. Allen, A review of the pathways of human exposure to poly-and perfluoroalkyl substances (PFASs) and present understanding of health effects, J. Exposure Sci. Environ. Epidemiol. 29 (2019) 131–147.
[5] F. Dixit, B. Barbeau, S.G. Mostafavi, M. Mohseni, Efficient removal of GenX (HFPO-DA) and other perfluorinated ether acids from drinking and recycled waters using anion exchange resins, J. Hazard. Mater. 384 (2020) 121261, https://doi.org/10.1016/j.jhazmat.2019.121261.
[6] P. Gao, J. Cui, Y. Deng, Direct regeneration of ion exchange resins with sulfate radical-based advanced oxidation for enabling a cyclic adsorption – regeneration treatment approach to aqueous perfluorooctanoic acid (PFOA), Chem. Eng. J. 405 (2021) 126698, https://doi.org/10.1016/j.cej.2020.126698.
[7] P. Wang, M. Zhang, Y. Lu, J. Meng, Q. Li, X. Lu, Removal of perfluoalkyl acids (PFAAs) through fluorochemical industrial and domestic wastewater treatment plants and bioaccumulation in aquatic plants in river and artificial wetland, Environ. Int. 129 (2019) 76–85.
[8] Z. Ren, U. Bergmann, T. Leiviskä, Reductive degradation of perfluorooctanoic acid in complex water matrices by using the UV/sulfite process, Water Res. 205 (2021) 117676, https://doi.org/10.1016/j.watres.2021.117676.
[9] J.N. Uwayezu, I. Carabante, T. Lejon, P. van Hees, P. Karlsson, P. Hollman, J. Kumpiene, Electrochemical degradation of per- and poly-fluoroalkyl substances using boron-doped diamond electrodes, J. Environ. Manag. 290 (2021) 112573, https://doi.org/10.1016/j.jenvman.2021.112573.
[10] S.S. Dalahmeh, N. Alziq, L. Ahrens, Potential of biochar filters for onsite wastewater treatment: effects of active and inactive biofilms on adsorption of per- and polyfluoroalkyl substances in laboratory column experiments, Environ. Pollut. 247 (2019) 155–164, https://doi.org/10.1016/j.envpol.2019.01.032.
[11] X. Xiao, B.A. Ulrich, B. Chen, C.P. Higgins, Sorption of poly- and perfluoroalkyl substances (PFASs) relevant to aqueous film-forming foam (AFFF)-impacted groundwater by biochars and activated carbon, Environ. Sci. Technol. 51 (2017) 6342–6351, https://doi.org/10.1021/acs.est.7b00970.
[12] B.O. Fagbayigbo, B.O. Opeolu, O.S. Fatoki, T.A. Akenga, O.S. Olatunji, Removal of PFOA and PFOS from aqueous solutions using activated carbon produced from Vitis vinifera leaf litter, Environ. Sci. Pollut. Res. 24 (2017) 13107–13120, https://doi.org/10.1007/s11356-017-8912-x.
[13] C.C. Murray, R.E. Marshall, C.J. Liu, H. Vatankhah, C.L. Bellona, PFAS treatment with granular activated carbon and ion exchange resin: comparing chain length, empty bed contact time, and cost, J. Water Process Eng. 44 (2021) 102342.
[14] R. Mukhopadhyay, B. Sarkar, K.N. Palansooriya, J.Y. Dar, N.S. Bolan, S.J. Parikh, C. Sonne, Y.S. Ok, Natural and engineered clays and clay minerals for the removal of poly- and perfluoroalkyl substances from water: state-of-the-art and future perspectives, Adv. Colloid Interface Sci. 297 (2021) 102537, https://doi.org/10.1016/j.cis.2021.102537.
[15] M.J. Klemes, Y. Ling, C. Ching, C. Wu, L. Xiao, D.E. Helbling, W.R. Dichtel, Reduction of a tetrafluoroterephthalonitrile-β-cyclodextrin polymer to remove anionic micropollutants and perfluorinated alkyl substances from water, Angew. Chem. 131 (2019) 12177–12181, https://doi.org/10.1002/ange.201905142.
[16] M. Ekesbo, Utility of bark chips for removal of fluorinated organic compounds in water samples at a hazardous waste management facility (2021).
[17] S. Deng, Y.Q. Zheng, F.J. Xu, B. Wang, J. Huang, G. Yu, Highly efficient sorption of perfluorooctane sulfonate and perfluorooctanoate on a quaternized cotton prepared by atom transfer radical polymerization, Chem. Eng. J. (2012) 154–160, https://doi.org/10.1016/j.cej.2012.04.005.
[18] S. Deng, L. Niu, Y. Bei, B. Wang, J. Huang, G. Yu, Adsorption of perfluorinated compounds on aminated rice husk prepared by atom transfer radical polymerization, Chemosphere 91 (2013) 124–130, https://doi.org/10.1016/j.chemosphere.2012.11.015.
[19] Lalhmunsiama, P.L. Gupta, H. Jung, D. Tiwari, S.H. Kong, S.M. Lee, Insight into the mechanism of Cd(II) and Pb(II) removal by sustainable magnetic biosorbent precursor to Chlorella vulgaris, J. Taiwan Inst. Chem. Eng. 71 (2017) 206–213, https://doi.org/10.1016/j.jtice.2016.12.007.
[20] Z. Cheng, Z. Gao, W. Ma, Q. Sun, B. Wang, X. Wang, Preparation of magnetic Fe3O4 particles modified sawdust as the adsorbent to remove strontium ions, Chem. Eng. J.l 209 (2012) 451–457, https://doi.org/10.1016/j.cej.2012.07.078.
[21] S. Fakhrian, H. Baseri, Production of a magnetic biosorbent for removing pharmaceutical impurities, Korean J. Chem. Eng. 37 (2020) 1541–1551, https://doi.org/10.1007/s11814-020-0523-4.
[22] C. Das, S. Singh, S. Bhakta, P. Mishra, G. Biswas, Bio-modified magnetic nanoparticles with Terminalia arjuna bark extract for the removal of methylene blue and lead (II) from simulated wastewater, Chemosphere 291 (2022) 132673, https://doi.org/10.1016/j.chemosphere.2021.132673.
[23] A.I. Adeogun, J.A. Akande, M.A. Idowu, S.O. Kareem, Magnetic tuned sorghum husk biosorbent for effective removal of cationic dyes from aqueous solution: isotherm, kinetics, thermodynamics and optimization studies, Appl. Water Sci. 9 (2019) 1–17, https://doi.org/10.1007/s13201-019-1037-2.
[24] M. Park, K.D. Daniels, S. Wu, A.D. Ziska, S.A. Snyder, Magnetic ion-exchange (MIEX) resin for perfluorinated alkylsubstance (PFAS) removal in groundwater: roles of atomic charges for adsorption, Water Res. 181 (2020) 115897, https://doi.org/10.1016/j.watres.2020.115897.
[25] G.R. Johnson, M.L. Brusseau, K.C. Carroll, G.R. Tick, C.M. Duncan, Global distributions, source-type dependencies, and concentration ranges of per-and polyfluoroalkyl substances in groundwater, Sci. Total Environ. 841 (2022) 156602.
[26] S.K. Lagergren, About the theory of so-called adsorption of soluble substances, Sven. Vetenskapsakad. Handingarl 24 (1898) 1–39.
[27] G. Blanchard, M. Maunaye, G. Martin, Removal of heavy metals from waters by means of natural zeolites, Water Res. 18 (1984) 1501–1507.
[28] S. Roginsky, Y.B. Zeldovich, The catalytic oxidation of carbon monoxide on manganese dioxide, Acta Phys. Chem. USSR 1 (1934) 554.
[29] W.J. Weber, J.C. Morris, Kinetics of adsorption on carbon from solution, J. Sanitary Eng. Division 89 (1963) 31–60.
[30] G.E. Boyd, A.W. Adamson, L.S. Myers Jr, The exchange adsorption of ions from aqueous solutions by organic zeolites. II. Kinetics1, J. American Chem. Society 69 (1947) 2836–2848.
[31] G. Rytwo, A.L. Zelkind, Evaluation of kinetic pseudo-order in the photocatalytic degradation of ofloxacin, Catalysts 12 (2021) 24.
[32] W.R. Vieth, K. Sladek, A model for diffusion in a glassy polymer, J. Colloid Sci. 20 (1965) 1014–1033.
[33] V.-P. Dinh, P.-T. Nguyen, M.-C. Tran, A.-T. Luu, N.Q. Hung, T.-T. Luu, H.A.T. Kiet, X.-T. Mai, T.-B. Luong, T.-L. Nguyen, H.T.T. Ho, D.-K. Nguyen, D.-K. Pham, A.-Q. Hoang, V.-T. Le, T.-C. Nguyen, HTDMA-modified bentonite clay for effective removal of Pb(II) from aqueous solution, Chemosphere 286 (2022) 131766, https://doi.org/10.1016/j.chemosphere.2021.131766.
[34] N.F. Campos, C.M.B.M. Barbosa, J.M. Rodríguez-Díaz, M.M.M.B. Duarte, Removal of naphthenic acids using activated charcoal: Kinetic and equilibrium studies, Adsorption Sci. Technol. 36 (2018) 1405–1421, https://doi.org/10.1177/0263617418773844.

[35] K. Vasanth Kumar, S. Sivanesan, Equilibrium data, isotherm parameters and process design for partial and complete isotherm of methylene blue onto activated carbon, J. Hazard. Mater. 134 (2006) 237–244, https://doi.org/10.1016/j.jhazmat.2005.11.002.
[36] Y. Gonen, G. Rytwo, Using the dual-mode model to describe adsorption of organic pollutants onto an organoclay, J. Colloid Interface Sci. 299 (2006) 95–101, https://doi.org/10.1016/j.jcis.2006.01.055.
[37] G. Rytwo, S. Levy, Y. Shahar, I. Lotan, A.L. Zelkind, T. Klein, C. Barak, Health protection using clay minerals: A case study based on the removal of BPA and BPS from water, Clays Clay Miner. 69 (2021) 641–653.
[38] H.N. Tran, S.J. You, A. Hosseini-Bandegharaei, H.P. Chao, Mistakes and inconsistencies regarding adsorption of contaminants from aqueous solutions: a critical review, Water Res. 120 (2017) 88–116, https://doi.org/10.1016/j.watres.2017.04.014.
[39] Z. Du, S. Deng, Y. Bei, Q. Huang, B. Wang, J. Huang, G. Yu, Adsorption behavior and mechanism of perfluorinated compounds on various adsorbents—a review, J. Hazard. Mater. 274 (2014) 443–454.
[40] P. Westreich, R. Mimna, J. Brewer, F. Forrester, The removal of short-chain and long-chain perfluoroalkyl acids and sulfonates via granular activated carbons: a comparative column study, Remediation J. 29 (2018) 19–26.
[41] B. Cantoni, A. Turolla, J. Wellmitz, A.S. Ruhl, M. Antonelli, Perfluoroalkyl substances (PFAS) adsorption in drinking water by granular activated carbon: influence of activated carbon and PFAS characteristics, Sci. Total Environ. 795 (2021) 148821, https://doi.org/10.1016/j.scitotenv.2021.148821.
[42] K. Raja, S. Verma, S. Karmakar, S. Kar, S.J. Das, K. Bartwal, Synthesis and characterization of magnetite nanocrystals, Crystal Res. Technol. 46 (2011) 497–500.
[43] K. Parveen, N. Kumar, L. Ledwani, Green synthesis of zinc oxide nanoparticles mediated from cassia renigera bark and detect its effects on four varieties of rice, ChemistrySelect 7 (2022) e202200415.
[44] J. Coates, Interpretation of infrared spectra, a practical approach, (2000).
[45] C. Cocozza, V. D'orazio, T.M. Miano, W. Shotyk, Characterization of solid and aqueous phases of a peat bog profile using molecular fluorescence spectroscopy, ESR and FT-IR, and comparison with physical properties, Organic Geochemistry 34 (2003) 49–60.
[46] O. Yayapao, T. Thongtem, A. Phuruangrat, S. Thongtem, CTAB-assisted hydrothermal synthesis of tungsten oxide microflowers, J. Alloys Compound. 509 (2011) 2294–2299, https://doi.org/10.1016/j.jallcom.2010.10.204.
[47] M.S. Shafeeyan, W.M.A.W. Daud, A. Houshmand, A. Shamiri, A review on surface modification of activated carbon for carbon dioxide adsorption, J. Anal. Appl. Pyrolysis 89 (2010) 143–151.
[48] N. Stevulova, J. Cigasova, A. Estokova, E. Terpakova, A. Geffert, F. Kacik, E. Singovszka, M. Holub, Properties characterization of chemically modified hemp hurds, Materials 7 (2014) 8131–8150.
[49] M. Mébarki, K. Hachem, M.K. Harche, Lignocellulosic fraction of the pericarps of the acorns of Quercus suber and Quercus ilex: isolation, characterization, and biosorption studies in the removal of copper from aqueous solutions, Polish J. Chem. Technol. 21 (2019).
[50] P.M. dos S. Silva, T.R. Fiaschitello, R.S. de Queiroz, H.S. Freeman, S.A. da Costa, P. Leo, A.F. Montemor, S.M. da Costa, Natural dye from Croton urucurana Baill. bark: Extraction, physicochemical characterization, textile dyeing and color fastness properties, Dyes Pigment. 173 (2020) 107953, https://doi.org/10.1016/j.dyepig.2019.107953.
[51] Y. Tian, X. Xu, Y. Zhao, X. Tang, T. Li, J. Sun, C. Li, A. Pan, Temperature-dependent FTIR study on self-assembly chiral liquid crystals through intermolecular hydrogen bonding, Thin Solid Films 284–285 (1996) 603–605, https://doi.org/10.1016/S0040-6090(95)08401-0.
[52] S.R. Kelemen, M. Afeworki, M.L. Gorbaty, P.J. Kwiatek, M. Sansone, C.C. Walters, A.D. Cohen, Thermal transformations of nitrogen and sulfur forms in peat related to coalification, Energy Fuels 20 (2006) 635–652.
[53] C.M. Popescu, C.M. Tibirna, C. Vasile, XPS characterization of naturally aged wood, Appl. Surface Sci. 256 (2009) 1355–1360, https://doi.org/10.1016/j.apsusc.2009.08.087.
[54] W. Cao, Z. Wang, Q. Zeng, C. Shen, 13C NMR and XPS characterization of anion adsorbent with quaternary ammonium groups prepared from rice straw, corn stalk and sugarcane bagasse, Appl. Surface Sci. 389 (2016) 404–410, https://doi.org/10.1016/j.apsusc.2016.07.095.
[55] Z. Du, S. Deng, Y. Bei, Q. Huang, B. Wang, J. Huang, G. Yu, Adsorption behavior and mechanism of perfluorinated compounds on various adsorbents-a review, J. Hazard. Mater. 274 (2014) 443–454, https://doi.org/10.1016/j.jhazmat.2014.04.038.
[56] R.L. Johnson, A.J. Anschutz, J.M. Smolen, M.F. Simcik, R.L. Penn, The adsorption of perfluorooctane sulfonate onto sand, clay, and iron oxide surfaces, J. Chem. Eng. Data 52 (2007) 1165–1170.
[57] M.J. Rosen, J.T. Kunjappu, Surfactants and Interfacial Phenomena, John Wiley & Sons, 2012.